Korean J. Chem. Eng., 40(4), 935-942 (2023)
DOI: 10.1007/s11814-022-1268-z

pISSN: 0256-1115
eISSN: 1975-7220

Experimental study rheological behavior of MWCNT (10%)-TiO_2 (90%)/SAE40 hybrid nano-lubricants (HNLs) post-processing of the results with response surface methodology (RSM)

Mohammad Hemmat Esfe*, Soheyl Alidoust, Saeed Esfandeh*, Davood Toghraie***,†, and Erfan Mohammadnejad Ardeshiri***

*Department of Mechanical Engineering, Imam Hossein University, Tehran, Iran
**School of Chemistry, Damghan University, Damghan 36716-41167, Iran
***Department of Mechanical Engineering, Khomeinishahr Branch, Islamic Azad University, Khomeinishahr, Iran
(*Received 6 April 2022 • Revised 14 August 2022 • Accepted 18 August 2022*)

Abstract−In this study, which was approached with an industrial approach, for the first time, the rheological behavior of hybrid nano-lubricants (HNLs) with the formulation MWCNT (10%)-TiO_2 (90%)/SAE40 was investigated experimentally, statistically and numerically. Nano-solution study conditions were performed in six solid volume fractions (=0.0625% to 1%) and a temperature range of T=25 to 50 °C. Quantitative statistics of laboratory studies show that the maximum and minimum viscosity of HNLs relative to the base oil increase and decrease by 29.6%, −13.40%, respectively. To predict the experimental data, to provide a correlation relationship and to establish a relationship between the target response and the effective variables, response surface methodology (RSM) with a three-point model and coefficient of determination 0.9986 was used.

Keywords: Hybrid Nano-lubricants (HNLs), Rheological Behavior, Response Surface Methodology, Experimental Study

INTRODUCTION

It is safe to say that nanostructures have created a huge revolution in various fields of science and researchers have done a great deal of research on this category of structures and this research is expanding every day [1-10]. Also, oils and lubricants play an important role in various industrial processes and researchers conduct research on them [11-14]. Hybrid nanofluids have become very popular due to their better thermophysical properties than conventional nanofluids. Due to the significant increase in heat generation and power loads in various applications, having coolants with superior thermal properties compared to conventional coolants is very much felt. To meet these thermal management needs, a new class of coolants, nanofluids, was introduced by Choi and Eastman [15] in 1995. Nanofluids are composed of nanometer-sized particles that are stably dispersed in conventional fluids. Following the pioneering work of Choi and Eastman [15], many researchers studied various aspects of the use of nanoparticles in various applications [16-18]. In these nanofluids, their properties can be changed by changing the type and ratio of the nanoparticles. The properties of nanofluids can be changed by changing several parameters such as SVF, nanoparticle diameter, nanoparticle shape, temperature, pH, surfactant and ultrasound time. But in the case of hybrid nanofluids, in addition to these parameters, the mixture ratio of nanoparticles and even the relative diameter also affect the thermophysical and rheological properties. The idea of using nanosolutions as a coolant in thermal discussions is because the presence of nanoparticles due to the higher thermal conductivity in the host fluid increases the thermal efficiency of conventional coolant [19,20]. More precisely, in the study [19], although the researchers used MWCNT (40%) and TiO_2 (60%) nanoparticles, only −7.29% reduction in viscosity was created in 10W40 fluid. Recently, a large number of studies were performed on the thermophysical properties of hybrid nanofluids [21-25]. Although viscosity is one of the most important parameters, the focus of most published articles is on thermal conductivity and heat transfer coefficient. However, some published papers have examined nanofluid viscosity (μ_{nf}) and related parameters [26-29]. Zadeh et al. [30] investigated the effect of temperature, SVF and size of nanoparticles on the μ_{nf} of water-based nanofluids containing alumina (Al_2O_3) and titania (TiO_2) nanoparticles. Their results show that nanofluids composed of TiO_2 nanoparticles show higher μ_{nf} than Al_2O_3 nanoparticles under the same conditions. The presence of nanoparticles enhances the viscosity of the HNL by 790% [22]. To this end, some researchers looked into predicting data and models [22,31]. In a research [32], the rheological behavior of titanium dioxide nanofluid based on ethylene glycol was investigated. They observed that the nanofluid has non-Newtonian shear-thinning behavior and can be described by the Ostwald de Waale model. Some experimental and correlation models were developed to predict changes in μ_{nf} [33,34], thermal conductivity [35,36] and rheological properties [37]. In this study, the rheological behavior of MWCNT (10%)-TiO_2 (90%)/SAE40 HNL was investigated using various laboratory and statistical methods. The purpose of this paper is to explain the performance of μ_{nf} based on

†To whom correspondence should be addressed.
E-mail: Toghraee@iaukhsh.ac.ir

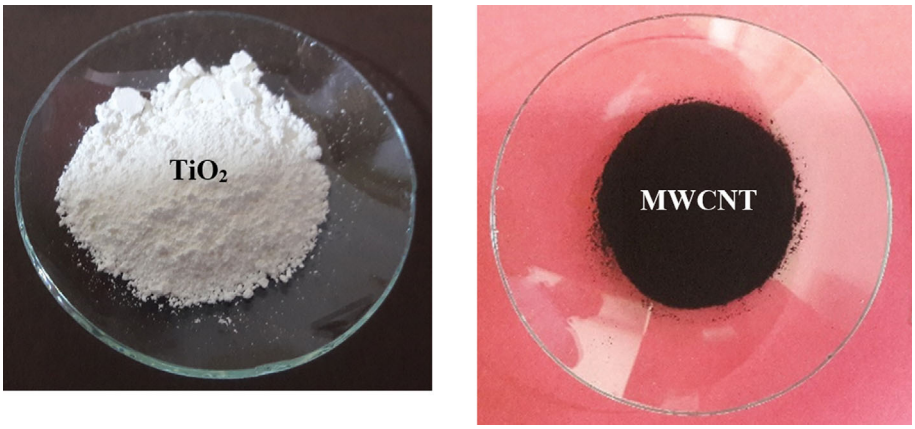

Fig. 1. TiO_2 and MWCNT nanopowders.

Table 1. Chemo-physical and morphological characteristics of nanoparticles

Nanoparticles	Purity	APS	SSA	Color	True density	Morphology
MWCNTs	>95 wt%	5-15 nm	233 m^2/g	Black	~2.1 g/cm^3	Cylindrical
TiO_2	99.9%	20 nm	10-45 m^2/g	White	4.23 g/cm^3	Nearly spherical

temperature, SVF and SR and determine the relationship between rheological behaviors using the RSM.

LABORATORY: EQUIPMENT AND MEASUREMENTS

In this study, MWCNT and TiO_2 nanopowders were used to prepare HNLs with SAE40 base fluid with a composition ratio of 10 : 90 (Fig. 1). One of the main reasons for using nanoparticles with this participation percentage is the expensiveness of MWCNT nanoparticles (10%). There are other studies available from Hammet's group that compare the percentage of different contributions of MWCNT-TiO_2 nanoparticles [16,19]. Compared to other studies, this study is more cost-effective based on the results of viscosity improvement and nanofluid preparation costs.

Table 1 reports the Chemo-physical and morphological characteristics of nanoparticles.

X-ray diffraction (XRD) pattern was used to study and check nanometer details, as well as to identify the structure and surface morphology of nanoparticles (Fig. 2). Based on Fig. 2, the MWCNT nanoparticle has a peak intensity of approximately 15,000 in the range of 20-40° and the TiO_2 nanoparticle has an approximate intensity of 5,000 in the same range.

The amount of required nanoparticles for the preparation of HNLs in SVFs was calculated from Eq. (1) [10]. Then, a digital scale with an accuracy of 0.001 g was used for weighing.

$$SVF = \frac{0.1\frac{W}{\rho}\Big|_{MWCNT} + 0.9\frac{W}{\rho}\Big|_{TiO_2}}{0.1\frac{W}{\rho}\Big|_{MWCNT} + 0.9\frac{W}{\rho}\Big|_{TiO_2} + \frac{W}{\rho}\Big|_{SAE40}} \times 100 \quad (1)$$

A magnetic stirrer was used for the homogenization and dispersion of nanoparticles in the base oil. Stability with a long duration without sediment was prepared as an important condition of HNLs.

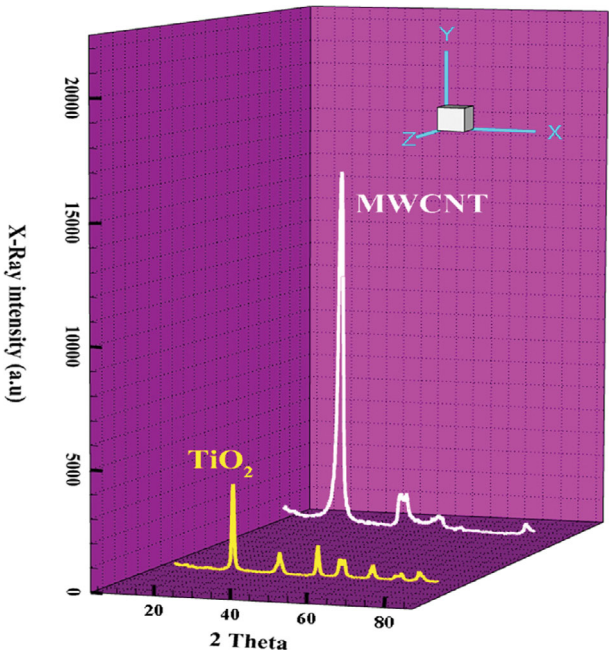

Fig. 2. XRD analysis of nanoparticles.

For this purpose, the ultrasonic vibrator was used to increase the quality and stability of HNLs. It is very difficult to obtain a uniform dispersion of HNL samples. Ultrasound plays an important role by altering the morphological and dimensional properties of nanomaterials. Chattopadhyay and Gupta [30] investigated the effect of ultrasonic intensity on different HNL samples. It was shown that increasing the ultrasonic intensity improves the HNL stability. Fig. 3 shows the stable HNLs at different SVFs for three weeks without observing sediment and sedimentation.

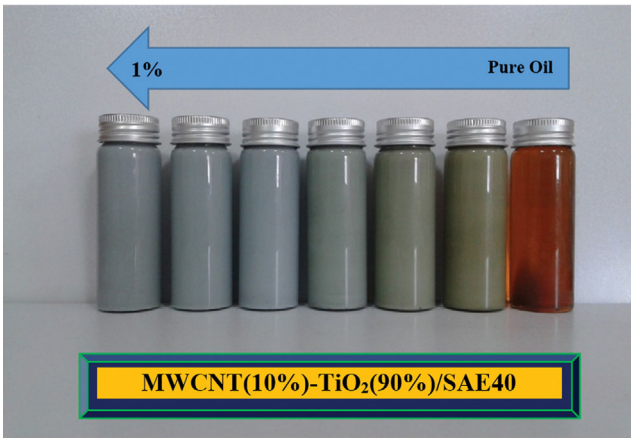

Fig. 3. Stability of HNLs at different SVFs.

1. Stability of HNLs

After preparing the HNLs, the important and necessary issue is to maintain its stability for a certain period of time. The stability of the HNL has been checked visually or as a density test. At first, the stability of prepared HNLs was checked by eye monitoring for two weeks. Then, by measuring the density test during the storage time of two weeks, changes in the apparent density of 0.1% were observed, which indicates the appropriate stability of the studied HNLs. Experimental data measurement is required to analyze the rheological behavior of HNLs. In the present study, the CAP2000+ viscometer designed in the United States was used to measure the μ_{nf} under laboratory conditions. To increase the accuracy of viscosity measurements, the calibration process was performed using SAE40 oil. Also, the measured data were repeated twice and then their average was recorded.

DISCUSSION

1. Rheological Behavior

1-1. Effect of SR

HNLs with different SVFs were used to investigate the rheological behavior (Fig. 4). The flow behavior of HNLs was compared using shear stress-SR and μ_{nf} curves. Based on the results of the shear stress-SR curve, HNLs have a different slope at each temperature, and since the slope in this diagram is equivalent to the μ_{nf}, as

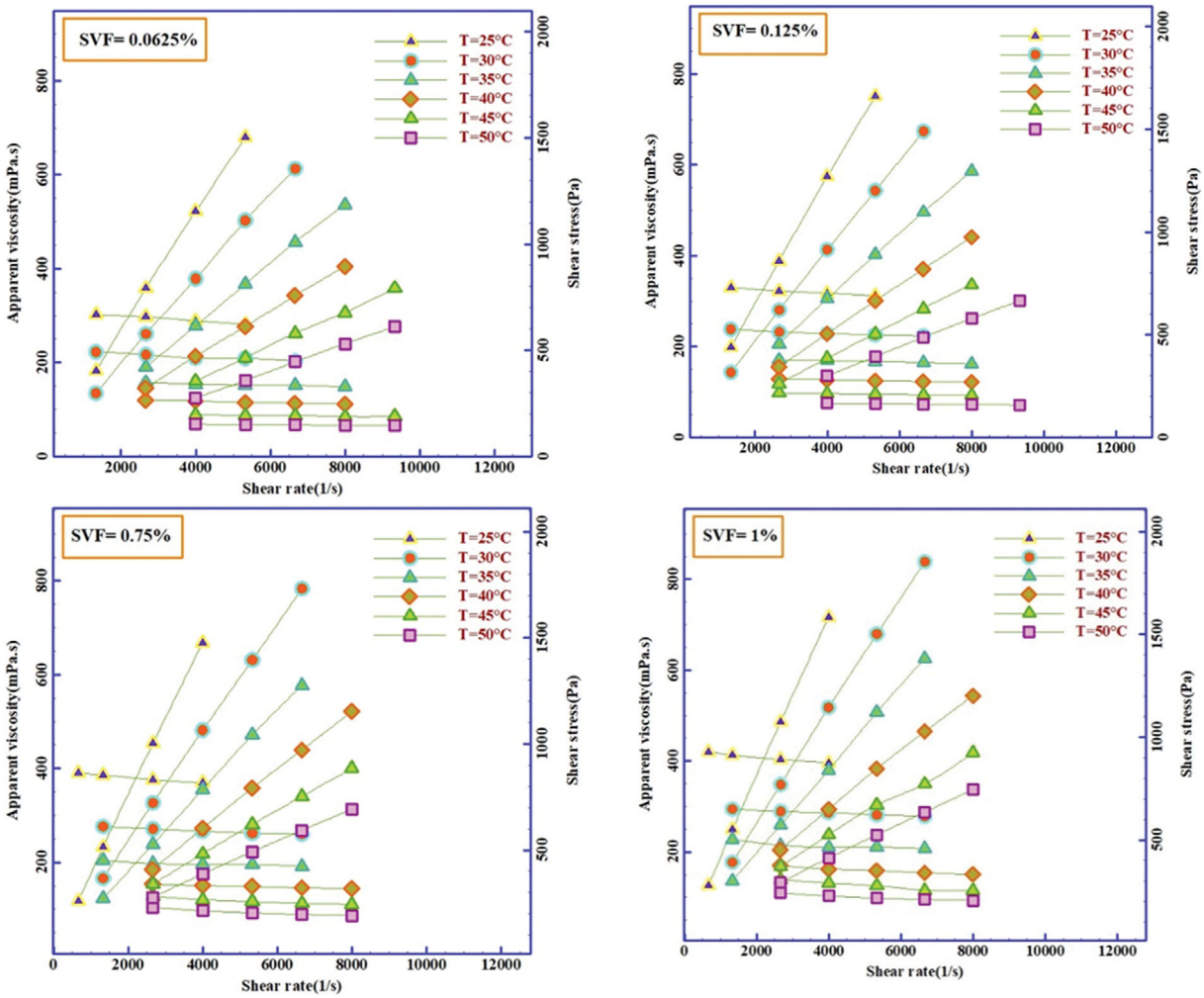

Fig. 4. Flow curve at different temperatures.

Table 2. Power-law index values at different SVFs and temperatures

HNLs		Power-law index (n)					
		T=25 °C	T=30 °C	T=35 °C	T=40 °C	T=45 °C	T=50 °C
MWCNT-TiO_2 (10 : 90)/SAE40	SVF=0.0625%	0.952	0.9442	0.9497	0.9349	0.9435	0.9463
	SVF=0.125%	0.9602	0.9607	0.9539	0.9524	0.9558	0.9431
	SVF=0.25%	0.9641	0.9648	0.9526	0.9418	0.9467	0.9389
	SVF=0.5%	0.9604	0.9545	0.9562	0.9565	0.9327	0.9077
	SVF=0.75%	0.9693	0.9618	0.9651	0.9411	0.8701	0.8315
	SVF=1%	0.9676	0.9671	0.9458	0.892	0.8153	0.8491

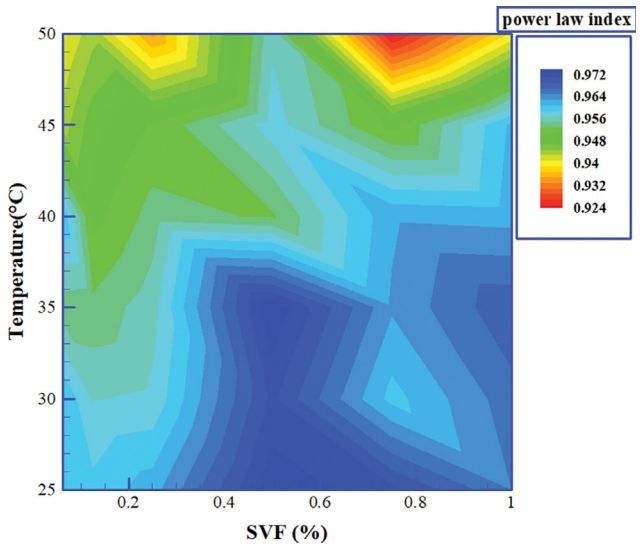

Fig. 5. The contour of the power-law index.

a result, it can be said that HNLs have non-Newtonian behavior [31,32]. It can also be said that because the μ_{nf} decreases with increasing SR, the result is a time-independent pseudo-plastic non-Newtonian HNL. As mentioned in Fig. 6, viscosity-SR and Shear stress-SR curves are merged together. To distinguish, the set of curves that have appeared in a descending form, is related to viscosity-SR, and on the other hand, the set of ascending curves shows shear stress-SR.

1-2. Power-law Index (n)

According to the power-law index contour shown in Fig. 5, HNL can be classified as non-Newtonian fluids [43], because according to Eq. (2) and Table 2, the values of n in different conditions were less than 1. The curve shows that the HNL in the most intense non-Newton state had n=0.8153.

$$\tau = m * SR^{n} \quad (2)$$

Based on Fig. 5 and according to the studies conducted [19,41], it can be said that the SAE40 fluid affected by the presence of MWCNT-TiO_2 nanoparticles exhibits non-Newtonian behavior. As shown, SAE40 base fluid alone has Newtonian behavior and is not suitable for lubrication purposes.

2. Viscosity Comparison

2-1. Relative μ_{nf} (μ_r)

In this section, using $\mu_r = \frac{\mu_{nf}}{\mu_{bf}}$ (Eq. (3)), the relative viscosity change (μ_r) is calculated and displayed as a contour according to Fig. 6. The contour of Fig. 6 clearly shows the effect of independent parame-

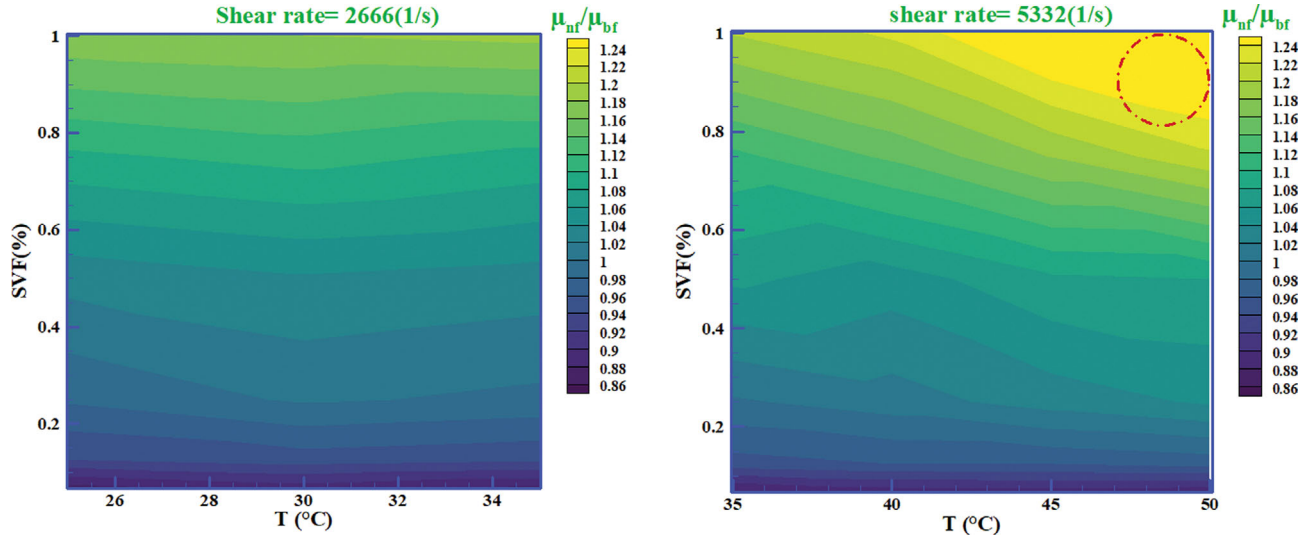

Fig. 6. μ_r contour at SR=2,666 and 5,332 s^{-1}.

Table 3. Statistical data on the percentage of μ_r changes

HNLs	SR (1/s)	T (°C)	$\mu_r=\frac{\mu_{nf}}{\mu_{bf}}$			
			SVF=0.0625%	SVF=0.125%	SVF=0.75%	SVF=1%
MWCNT-TiO_2 (10 : 90)/SAE40	2,666 (200 rpm)	25	0.866 (−13.40%)	0.939	1.095	1.174
		30	0.885	0.95	1.107	1.18
		35	0.87	0.943	1.093	1.186
	5,332 (400 rpm)	35	0.868	0.952	1.115	1.201
		40	0.884	0.960	1.144	1.224
		45	0.886	0.962	1.181	1.276
		50	0.882	0.969	1.216	1.296 (+29.60%)

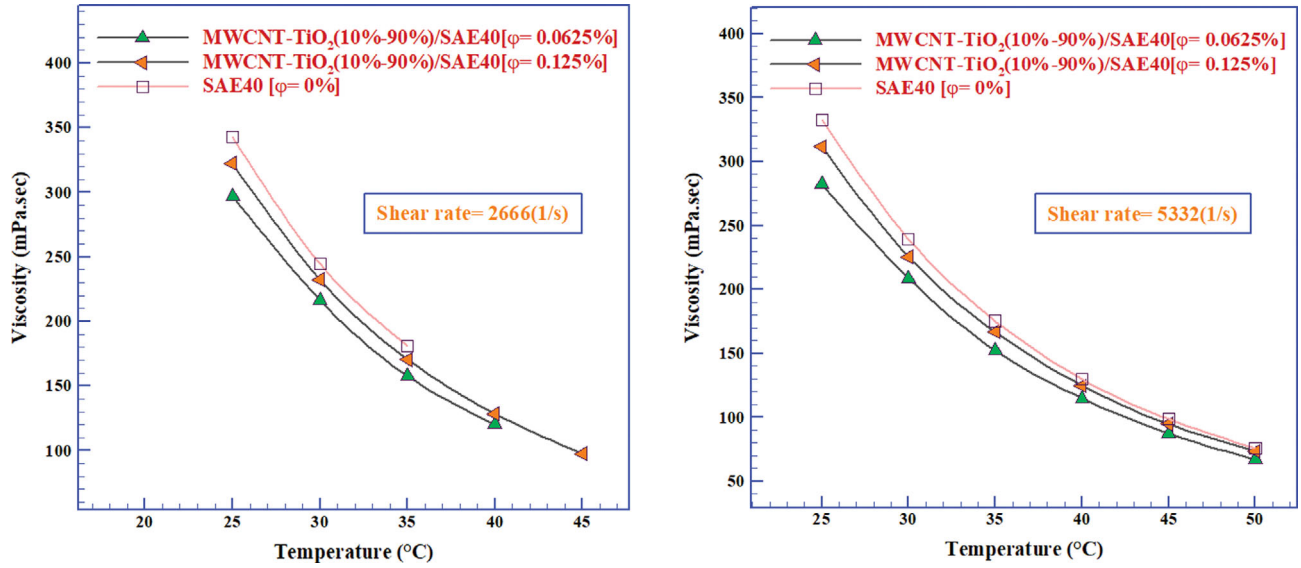

Fig. 7. Viscosity difference between HNL and base fluid at SR=2,666 and 5,332 s^{-1} and different SVFs.

ters of temperature and SVF on the dependent variable of viscosity. So that in the specified area (red circle), the maximum increase in viscosity occurs in the temperature range of 45-50 °C at SR=5,332 s^{-1}. On the other hand, this increase was occurring at SVF higher than 0.8%; so, it can be said that viscosity has a direct relationship with the SVF. The accumulation of nanoparticles in the fluid, more than the mentioned concentration range, reduces the fluidity of the HNL and the optimal control of the viscosity and will increase the viscosity more than expected.

According to the exact numerical values reported in Table 3, −13.40% was the maximum viscosity decrease and +29.60% was the maximum viscosity increase, which according to the table occurred in different conditions. The μ_r results are reported in Table 3.

2-2. μ_{nf}→T Curve

Comparing the difference of μ_{nf} with SAE40 Oil shows that after adding nanoparticles to the base-oil, it has experienced a severe drop in viscosity. This behavior indicates the selection of suitable conditions of SVF, temperature and SR to prepare the HNL According to Fig. 7, the controlled decrease in viscosity occurred in both SVFs of 0.0625% and 0.125%. But SVF=0.0625% is preferable both in terms of low production cost and initial viscosity drop at T= 25 °C compared to SVF=0.125%. The presence of nanoparticles with the mentioned SVF in the fluid acts like a bearing and reduces the viscosity of the fluid.

Table 4. Comparison of the difference between the μ_{nf} and μ_{bf} at different SRs and SVFs

SR (s^{-1})	T (°C)	$\Delta(\mu_{n-b})_f$|SVF=0.0625%	$\Delta(\mu_{n-b})_f$|SVF=0.125%
		MWCNT-TiO_2 (10 : 90)/SAE40	
2,666	25 °C	−45.9 (−13.37%)	−20.60
	30 °C	−28.10	−12.20
	35 °C	−23.40	−10.30
5,332	40 °C	−15.00	−5.10
	45 °C	−11.20	−3.70
	50 °C	−8.90	−2.30 (−3.03%)

According to Table 4, the maximum drop in viscosity at SR= 2,666 s^{-1}, T=25 °C and SVF=0.0625 was equal to −13.37%. On the other hand, minimum drop in viscosity SR=5,332 s^{-1}, T=50 °C and SVF=0.125 is reported as −3.03%.

Table 5. ANOVA for response surface reduced cubic model

Analysis of variance table [Partial sum of squares - Type III]						
	Sum of		Mean	F	p-value	
Source	Squares	df	Square	Value	Prob>F	
Model	58.99	11	5.36	10,273.42	<0.0001	Significant
A-T	6.38	1	6.38	12,216.15	<0.0001	
B-SVF	0.051	1	0.051	96.80	<0.0001	
C-SR	0.066	1	0.066	125.67	<0.0001	
BC	0.022	1	0.022	41.47	<0.0001	
A^2	0.63	1	0.63	1,202.82	<0.0001	
B^2	0.031	1	0.031	60.29	<0.0001	
ABC	7.724E-003	1	7.724E-003	14.80	0.0002	
A^2B	6.103E-003	1	6.103E-003	11.69	0.0008	
A^2C	3.509E-003	1	3.509E-003	6.72	0.0104	
A^3	2.170E-003	1	2.170E-003	4.16	0.0431	
B^3	0.057	1	0.057	110.14	<0.0001	
Residual	0.085	162	5.220E-004			
Cor total	59.08	173				
Transform: Power, Lambda: 0.28, Constant: 0						

IMPRACTICAL RESULTS

1. Correlation Model of the RSM

The RSM was used for mathematical modeling of the relationship between the dependent variable and the independent variable. RSM is one of the favorite methods of researchers to model different parameters in laboratory and industrial scale. In this method, one or more influential independent variables are used. RSM is usually used in modeling, designing, manufacturing and optimizing processes. This method deals with modeling with different orders, including the first order, second order, etc. In this study, by performing regression analysis and processing the results on input and output experimental data, modeling is done and then from the three-variable-three-degree nonlinear mathematical relationship resulting from the transfer function Transform: Power, Lambda: 0.28, Constant: 0 for Prediction of laboratory values was presented. According to Table 5, parameter A is the temperature model, parameter B is equivalent to SVF and C is the SR.

The criteria of probability value (p-value), coefficient of variation (C.V%) and coefficient of determination (R^2) are used to measure the quality of the model. The coefficient of variation is an important factor in checking the accuracy of the correlation model and the quality of the products. This index measures the reliability and repeatability of the model with a maximum allowed of less than 10%. Also, the values of R^2, Adj-R^2, and Pred-R^2 are reported as 0.9986, 0.9985, and 0.9983, respectively, based on Table 6, which are very appropriate, accurate, and confirming values for the model used in the RSM.

Table 6. Determined model accuracy

Std. Dev.	0.023	R-Squared	0.9986
Mean	4.16	Adj R-Squared	0.9985
C.V. %	0.55	Pred R-Squared	0.9983
PRESS	0.099	Adeq Precision	362.599

$$(\mu_{nf})^{0.28} = +8.61560 - 0.20625\,T + 1.12502\,SVF - 1.65182E\text{-}005\,SR + 2.00653E\text{-}005\,SR*SVF + 2.74830E\text{-}003\,T^2 - 1.59558\,SVF^2 - 9.47270E\text{-}007\,T*SR*SVF + 5.53858E\text{-}005\,T^2*SVF + 4.45720E\text{-}009\,T^2*SR - 1.54968E\text{-}005\,T^3 + 0.90259\,SVF^3 \quad (3)$$

In Fig. 8, the well-modeled data correlates with the experimental data, indicating the acceptable validity of the model-function relationship.

CONCLUSION

The behavior of HNL rheology was studied to recognize the

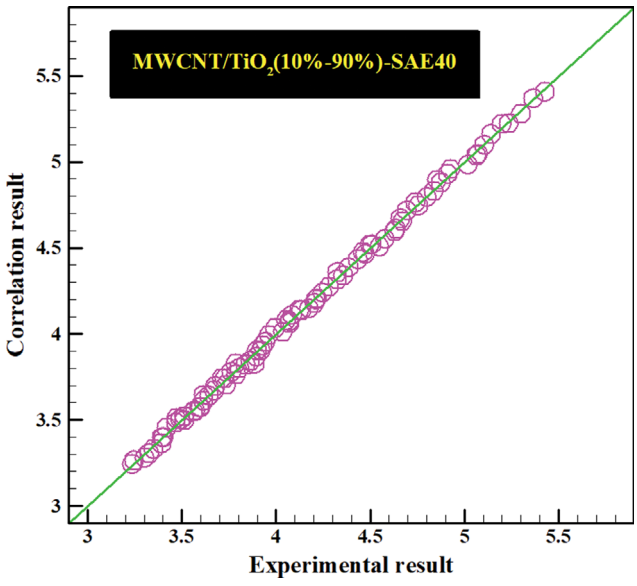

Fig. 8. Correlation of modeled data with laboratory data.

industry and its application in the field of related industries. The behavior of HNLs was investigated by laboratory and statistical analyses. This paper aims to build a stable HNL based on nanotechnology and to provide optimal functional conditions. The main results are reported in the following cases:

- The μ_{nf} in different laboratory conditions based on behavioral analysis was determined as pseudo-plastic non-Newtonian.
- Quantitative results of experimental studies show that the maximum and minimum viscosity of HNLs compared to the base oil have increased and decreased by 29.60% and −13.40%, respectively.
- Using the RSM, the experimental data were modeled with a three-variable-three-degree model and the transfer function Transform: Power, Lambda: 0.28, Constant: 0, and then the nonlinear mathematical relation of the target response with a coefficient of determination of 0.9986 was presented.

CONFLICT OF INTEREST STATEMENT

The authors declare that they have no known competing financial interests or personal relationships that could have appeared to influence the work reported in this paper.

NOMENCLATURE

ρ : density
n : power-law coefficient
T : temperature
$\dot{\gamma}$: shear rate
τ : shear stress
m : consistency index
μ_{pre} : predicted dynamic viscosity
w : weight percent
μ_{exp} : laboratory dynamic viscosity
μ_{bf} : dynamic viscosity of the base fluid
φ : volume fraction
μ_{rel} : relative dynamic viscosity
ANN : artificial neural network
APS : average particle size
EG : ethylene glycol
MOD : margin of deviation
MWCNT : multi-walled carbon nanotube
RSM : response surface methodology
SEM : scanning electron microscope
TEM : transmission electron microscope
XRD : X-ray diffraction

REFERENCES

1. M. Bahmani, M. Taherikalani, M. Khaksarian, M. Rafieian-Kopaei, B. Ashrafi, M. Nazer and M. Alizadeh, *J. Pharm. Negat.*, **10**(1), 16 (2019).
2. J. He, P. Xu, R. Zhou, H. Li, H. Zu, J. Zhang and F. Wang, *Adv. Electron. Mater.*, **8**(4), 2100997 (2022).
3. N. U. Saqib, R. Adnan and I. Shah, *Iran. J. Chem. Chem. Eng.*, **40**(4) (2021).
4. Z. Azin and Z. Pourghobadi, *Iran. J. Chem. Chem. Eng.*, **40**(4) (2021).
5. M. H. Esfe and M. R. Sarlak, *J. Mol. Liq.*, **242**, 326 (2017).
6. P. Suanto, A. P. Usman, A. Saggaff, M. Ismail and N. H. A. Khalid, *IJIRSS*, **5**(1), 18 (2022).
7. R. Bakhshkandi and M. Ghoranneviss, *JRSET*, **7**(4), 1 (2019).
8. S. Piramoon, P. Aberoomand Azar, M. Saber Tehrani and S. Mohamadi Azar, *IJCCE*, **40**(5), 1541 (2021).
9. S. Alidoust, M. Zamani and M. Jabbari, *IJC*, **10**(4), 295 (2020).
10. S, Rahimnejad and T. M. Bikhof, *J. Chem. Health Risks.*, **6**(3), 203 (2016).
11. C. U. I. Xin, L. I. Changhe, D. I. N. G. Wenfeng, C. H. E. N. Yun, M. A. O. Cong, X. U. Xuefeng and S. Sharma, *CJA* (2021).
12. M. Liu, C. Li, Y. Zhang, Q. An, M. Yang, T. Gao and S. Sharma, *Front. Mech. Eng.*, **16**(4), 649 (2021).
13. A. B. W. Putra, *IJCCTS*, **8**(2), 9 (2020).
14. X. Wu, C. Li, Z. Zhou, X. Nie, Y. Chen, Y. Zhang and S. Sharma, *Int. J. Adv. Manuf. Technol.*, **117**(9), 2565 (2021).
15. S. U. Choi and J. A. Eastman, Argonne, IL (United States) (1995).
16. M. H. Esfe, A. A. A. Arani, M. R. Madadi and A. Alirezaie, *J. Mol. Liq.*, **260**, 229 (2018).
17. M. H. Esfe and A. A. A. Arani, *J. Mol. Liq.*, **259**, 227 (2018).
18. M. Sheikholeslami and S. A. Farshad, *Renew. Energy*, **171**, 1128 (2021).
19. M. H. Esfe, D. Toghraie, S. Alidoust, S. Esfandeh and E. M. Ardeshiri, *Colloids Surf. A Physicochem. Eng. Asp.*, **647**, 129078 (2022).
20. M. Hemmat Esfe, *J. Therm. Anal. Calorim.*, **127**(3), 2125 (2017).
21. O. Hozien, W. M. El-Maghlany, M. M. Sorour and Y. S. Mohamed, *J. Mol. Liq.*, **334**, 116128 (2021).
22. Y. M. Chu, M. Ibrahim, T. Saeed, A. S. Berrouk, E. A. Algehyne and R. Kalbasi, *J. Mol. Liq.*, **333**, 115969 (2021).
23. A. Asadi, I. M. Alarifi and L. K. Foong, *J. Mol. Liq.*, **307**, 112987 (2020).
24. A. Z. Akhtar, M. M. Rahman, K. Kadirgama and M. A. Maleque, *Int. J. Automot. Eng.*, **17**(3), 8224 (2020).
25. N. K. Deenesh, A. Mahmood, G. Kadir, K. Hasnan and N. Nafarizal, *J. Phys. Conf. Ser.*, **1878**, 012017 (2021).
26. M. Klazly and G. Bognár, *ICHMT*, **135**, 106054 (2022).
27. A. Dezfulizadeh, A. Aghaei, A. H. Joshaghani and M. M. Najafizadeh, *Powder Technol.*, **389**, 215 (2021).
28. S. Alidoust, F. AmoozadKhalili and S. Hamedi, *Colloids Surf. A Physicochem. Eng. Asp.*, **645**, 128625 (2022).
29. Z. An, Y. Zhang, Q. Li, H. Wang, Z. Guo and J. Zhu, *Powder Technol.*, **328**, 199 (2018).
30. A. D. Zadeh and D. Toghraie, *J. Therm. Anal. Calorim.*, **131**(2), 1449 (2018).
31. M. H. Esfe, H. Rostamian and M. R. Sarlak, *J. Mol. Liq.*, **254**, 406 (2018).
32. D. Cabaleiro, M. J. Pastoriza-Gallego, C. Gracia-Fernández, M. M. Piñeiro and L. Lugo, *Nanoscale Res. Lett.*, **8**(1), 1 (2013).
33. A. H. Saeedi, M. Akbari and D. Toghraie, *Phys. E: Low-Dimens. Syst. Nan.*, **99**, 285 (2018).
34. B. C. Sahoo, R. S. Vajjha, R. Ganguli, G. A. Chukwu and D. K. Das, *Pet. Sci. Technol.*, **27**(15), 1757 (2009).
35. A. B. Colak, *Int. J. Energy Res.*, **45**(2), 2912 (2021).
36. R. Bakhtiari, B. Kamkari, M. Afrand and A. Abdollahi, *Powder*

Technol., **385**, 466 (2021).
37. D. Sawicka, J. T. Cieśliński and S. Smolen, *J. Nanomater.*, **10**(8), 1487 (2020).
38. P. Chattopadhyay and R. B. Gupta, *Int. J. Pharm.*, **228**(1-2), 19 (2001).
39. A. Haldar, S. Chatterjee, A. Kotia, N. Kumar and S. K. Ghosh, *ICHMT*, 116, 104723 (2020).
40. B. El Far, S. M. M. Rizvi, Y. Nayfeh and D. Shin, *Int. J. Heat Mass Transf.*, **156**, 119789 (2020).
41. Y. M.Chu, M. Ibrahim, T. Saeed, A. S. Berrouk, E. A. Algehyne and R. Kalbasi, *J. Mol. Liq.*, **333**, 115969 (2021).
42. M. H. Esfe, D. Toghraie, S. Alidoust, F. Amoozad and E. M. Arsdeshiri, *Heliyon*, e11561 (2022).